

ACKNOWLEDGMENTS

The authors would like to thank I. R. Williams for his aid in counting the irradiated samples. The cooperation of the tandem Van de Graaff accelerator crew is also gratefully acknowledged.

*Research sponsored by the U. S. Atomic Energy Commission under contract with Union Carbide Corporation.

†Present address: Trinity University, San Antonio, Texas 78212.

¹G. Breit and M. E. Ebel, *Phys. Rev.* **103**, 679 (1956); M. E. Ebel, *ibid.* **103**, 958 (1956); G. Breit and M. E. Ebel, *ibid.* **104**, 1030 (1956); G. Breit, in *Handbuch der Physik*, edited by S. Flügge (Springer-Verlag, Berlin, Germany, 1959), Vol. 41, Pt. 1; G. Breit, *Phys. Rev.* **135**, B1323 (1964); G. Breit, K. W. Chun, and H. G. Wahsweiler, *ibid.* **133**, B403 (1964).

²L. C. Becker and J. A. McIntyre, *Phys. Rev.* **138**, B339 (1965).

³R. M. Gaedke, K. S. Toth, and I. R. Williams, *Phys. Rev.* **141**, 996 (1966).

⁴T. Kammuri and R. Nakasima, in *Proceedings of the Third International Conference on Reactions between Complex Nuclei, Asilomar, 1963*, edited by A. Ghiorso, R. M. Diamond, and H. E. Conzett (University of California Press, Berkeley, California, 1963); T. L. Abelishvili, *Zh. Eksperim. i Teor. Fiz.* **40**, 1440 (1961) [transl.: *Soviet Phys.-JETP* **13**, 1010 (1961)].

⁵P. J. A. Buttle and L. J. B. Goldfarb, *Nucl. Phys.* **78**, 409 (1966).

⁶L. J. B. Goldfarb and J. W. Steed, *Nucl. Phys.* **A116**, 321 (1968).

⁷T. Sawaguri and W. Tobocman, *J. Math. Phys.* **8**, 2223 (1967).

⁸F. Schmittroth, W. Tobocman, and A. A. Golestaneh, *Phys. Rev. C* **1**, 337 (1970).

⁹H. L. Reynolds, D. W. Scott, and A. Zucker, *Phys. Rev.* **95**, 671 (1954).

¹⁰S. K. Allison and S. D. Warshaw, *Rev. Mod. Phys.* **25**, 779 (1953).

¹¹J. P. Schiffer, G. C. Morrison, R. H. Siemssen, and B. Zeidman, *Phys. Rev.* **164**, 1274 (1967).

¹²S. Cohen and D. Kurath, *Nucl. Phys.* **A101**, 1 (1967).

¹³H. L. Reynolds and A. Zucker, *Phys. Rev.* **101**, 166 (1956).

¹⁴J. C. Hiebert, J. A. McIntyre, and J. G. Couch, *Phys. Rev.* **138**, B346 (1965).

¹⁵G. Breit, *Proc. Nat. Acad. Sci. U.S.A.* **67**, 849 (1967).

¹⁶C. Shakin, L. L. Foldy, and P. Zilsel, private communication.

Quasielastic Electron Scattering and Pion Electroproduction from C^{12†}

K. C. Stanfield,* C. R. Canizares,‡ W. L. Faissler,§ and F. M. Pipkin
Cyclotron Laboratory, Harvard University, Cambridge, Massachusetts 02138

(Received 27 October 1970)

This paper reports measurements made at the Cambridge Electron Accelerator of the electron-carbon scattering cross section at incident energies of 1, 1.5, 2.25, 3, and 4 GeV and at lab angles of 8.5, 12, and 18°. The measurements included quasielastic scattering and inelastic scattering through the region of the first pion-nucleon resonance. The data are compared with a spectrum generated by summing the known elastic cross section, the known cross sections for excitation of nuclear levels, and a theoretical expression for quasielastic scattering based on the Fermi model for the nucleus. The agreement is satisfactory. The meson electroproduction cross section was derived by subtracting the above calculated spectrum from the data. The total equivalent photoabsorption cross section is consistent with the cross section expected for 12 independent nucleons; the existing Fermi-model calculation does not, however, correctly predict the shape of the electron momentum spectrum. The data are also used to test the Drell-Schwartz sum rule.

I. INTRODUCTION

Many experimental and theoretical studies have been made of electron scattering from carbon.^{1,2} There are several reasons for this attention. The

carbon nucleus is quite interesting from the standpoint of nuclear physics; thus, much of the experimental work has emphasized the elastic and nuclear level regions of the momentum spectrum.^{3,4} Because of its accessibility and simplicity the car-

bon nucleus has been used extensively as a target in experiments performed to test quantum electrodynamics. It has been shown by Drell and Walecka⁵ that the form factors required to remove the nuclear-physics effects in the electrodynamics experiments can be measured by studying the electron scattering from carbon as a function of the four-momentum transfer and the energy loss to the nucleus. Czyz and Gottfried⁶ have shown that two-nucleon correlations in the nucleus would lead to a high-energy loss tail on the outgoing electron momentum spectrum for quasielastic scattering. In order to investigate these two-body correlations, the quasielastic scattering must be understood in some detail. Walecka⁷ and Moniz⁸ have conjectured that it may be possible to study nucleon-nucleon resonance ($N-N^*$) reactions by using electron scattering to produce N^* 's in the nucleus. At fixed q^2 , the form-factor variation with atomic number could give information about the total $N-N^*$ cross section. Such conjectures are predicated on a detailed understanding of the nucleon momentum distribution in the nucleus.

This paper reports a new study of electron scattering from carbon using high-energy electrons from the Cambridge Electron Accelerator. Measurements were made at incident energies of 1, 1.5, 2.25, 3, and 4 GeV and at lab angles of 8.5, 12, and 18°. They included quasielastic scattering and inelastic scattering through the first pion-nucleon resonance. This paper also reports the results of a final analysis of some previously reported data⁹ with incident energies up to 5 GeV and scattering angles down to 3.3°.

This paper treats in sequence the theory behind the experiment, the known data concerning electron scattering from carbon, the procedure used in taking data, the method of data reduction and the results of the experiment.

II. THEORETICAL BACKGROUND

A. Notation

The theory for electron-nucleus scattering has been studied by many authors and several excellent reviews are available.¹⁻⁴ We shall give here a brief summary of the concepts used in the analysis of the data for this experiment.

Table I summarizes the notation that will be used in this paper. Figure 1 shows the generalized Feynman diagram for electron scattering in the one-photon-exchange approximation. The metric is chosen so that the four-momentum transfer squared is positive. That is

$$q^2 = (\vec{q})^2 - \omega^2 > 0.$$

The electron will always be assumed to be ex-

tremely relativistic so that $\beta = 1$; the electron mass will be neglected wherever possible.

B. General Formalism

It has been shown by Drell and Walecka⁵ that in the one-photon-exchange approximation, if only the final electron is observed, the cross section depends on two form factors, $W_1(q^2, q \cdot P_3)$ and $W_2(q^2, q \cdot P_3)$. The expression for the cross section is

$$\frac{d^2\sigma}{d\Omega_f d\epsilon_f} = \frac{\sigma_M}{M_T} [W_2(q^2, q \cdot P_3) + 2 \tan^2 \frac{1}{2} \theta W_1(q^2, q \cdot P_3)]. \quad (1)$$

Here σ_M is the Mott cross section

$$\sigma_M = (\alpha^2 \cos^2 \frac{1}{2} \theta) / (4\epsilon_i^2 \sin^4 \frac{1}{2} \theta), \quad (2)$$

and α is the fine-structure constant. In the lab system

$$q \cdot P_3 = \omega M_T, \quad (3)$$

and thus the form factors are functions of only the

TABLE I. Definition of the variables used in this paper.

p_1 :	four-momentum of incident electron having the value (ϵ_i, \vec{p}_i) in the lab.
p_2 :	four-momentum of scattered electron having the value (ϵ_f, \vec{p}_f) in the lab.
P_3 :	four-momentum of target particle having the value (E_T, \vec{P}_T) in the lab.
P_4 :	four-momentum of the recoil particle having the value (E_f, \vec{P}_f) in the lab.
$M_T = (-P_3^2)^{1/2}$:	mass of the target.
$M_f = (-P_4^2)^{1/2}$:	mass of recoiling particle.
m_e :	electron mass.
m_π :	pion mass.
M :	nucleon mass.
$q = (\omega, \vec{q}) = P_1 - P_2$:	four-momentum transfer to the target.
θ :	polar angle of scattered electron relative to incident electron in the laboratory.
ξ_1 :	polar angle of target particle relative to incident electron in the laboratory.
ξ_2 :	angle between \vec{p}_f and \vec{P}_T .
v_T :	velocity of target nucleon divided by the velocity of light.
M_{33} :	1236 MeV.
M_{13} :	1525 MeV.
Γ_{33} :	120 MeV.
Γ_{13} :	115 MeV.
K :	equivalent photon energy $(= \omega - q^2/2M_T)$.
k_F :	Fermi momentum of the nucleons.
Q :	ratio of $ \vec{q} $ to k_F ($ \vec{q} /k_F$).
M^* :	effective nucleon mass.
Z :	atomic number.
N :	neutron number.
A :	$Z + N$.
μ_p :	proton magnetic moment.
μ_n :	neutron magnetic moment.

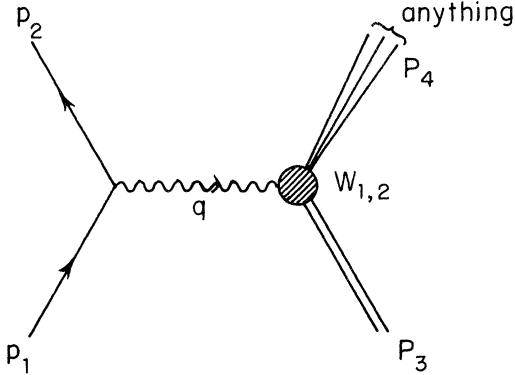


FIG. 1. Generalized Feynman diagram for electron scattering in the one-photon-exchange approximation.

invariant four-momentum transfer q^2 and the energy loss ω .

For elastic scattering from a spin-zero target such as carbon

$$W_1 = 0, \quad (4)$$

$$W_2 = Z^2 |F(q^2)|^2 \frac{M_T^2}{E_f} \delta(E_T - E_f + \omega). \quad (5)$$

The elastic scattering cross section is given by

$$\frac{d\sigma_{el}}{d\Omega_f} = \int_{\text{elastic peak}} \frac{d^2\sigma}{d\Omega_f d\epsilon_f} d\epsilon_f, \quad (6)$$

$$= (Z^2 \sigma_M / \eta) |F(q^2)|^2, \quad (7)$$

where

$$\eta = 1 + (2\epsilon_i / M_T) \sin^2 \frac{1}{2} \theta. \quad (8)$$

This procedure can be generalized to cover the case where "elastic" scattering includes level excitation and quasielastic scattering. The "elastic" scattering cross section is given by

$$\frac{d\sigma_{\text{"el"}}}{d\Omega_f} = \int_{\text{"elastic"}} \frac{d^2\sigma}{d\Omega_f d\epsilon_f} d\epsilon_f, \quad (9)$$

where the integration is over the elastic peak, the nuclear levels and the quasielastic scattering. The contribution due to a given energy level where the mass of the final nucleon system is M_f can be written in the form

$$\frac{d\sigma}{d\Omega_f} = \frac{Z^2 \sigma_M}{\eta} [w_2(q^2) + 2w_1(q^2) \tan^2 \frac{1}{2} \theta]. \quad (10)$$

The energy of the scattered electron is then given by the equation

$$\epsilon_f = \frac{\epsilon_i - (M_f^2 - M_T^2) / 2M_T}{1 + (2\epsilon_i / M_T) \sin^2 \frac{1}{2} \theta}. \quad (11)$$

Since the nucleus makes transitions between states of definite angular momentum and parity,

it is useful to make a multipole analysis of the nuclear current operator, as has been done by de Forest and Walecka.⁴ In order to carry out the analysis, several assumptions are made. Only one-photon exchange is assumed, and nuclear-recoil effects are neglected in the nuclear matrix elements. The only effect of nuclear recoil is included in the factor η . The cross section as given by de Forest and Walecka may be written

$$\frac{d\sigma}{d\Omega_f} = \frac{4\pi\sigma_M}{\eta} \left[\frac{q^4}{(\tilde{q})^4} F_C^2(q^2) + \left(\frac{q^2}{2(\tilde{q})^2} + \tan^2 \frac{1}{2} \theta \right) F_T^2(q^2) \right]. \quad (12)$$

F_C and F_T are the Coulomb and transverse form factors, respectively. F_C describes those transitions where zero units of angular momentum are carried along the direction of \tilde{q} ; F_T describes those transitions where ± 1 units of angular momentum are carried along \tilde{q} . The transverse form factor is comprised of two noninterfering amplitudes called "electric" and "magnetic," which generate transitions of parity $(-1)^J$ and $-(-1)^J$, respectively. In terms of F_C^2 and F_T^2

$$w_1 = \frac{2\pi}{Z^2} F_T^2, \quad (13)$$

$$w_2 = \frac{2\pi}{Z^2} \frac{q^2}{\tilde{q}^2} \left(F_T^2 + 2 \frac{q^2}{\tilde{q}^2} F_C^2 \right). \quad (14)$$

Thus, w_1 is entirely transverse, while w_2 is part Coulomb and part transverse.

C. Elastic Scattering

Since carbon is a spin-zero nucleus, only the Coulomb form factor contributes to elastic scattering. This form factor is the Fourier transform of the spherically symmetric charge distribution. Hence

$$\frac{d\sigma}{d\Omega} = \frac{Z^2 \sigma_M}{\eta} F^2(q^2). \quad (15)$$

At present, the consensus of the literature¹⁰⁻¹⁵ is that the ground-state charge distribution for carbon is best represented by the parabolic-well shell-model distribution

$$\rho(r) = \rho(0) (1 + \alpha r^2 / a^2) e^{-r^2 / a^2}, \quad (16)$$

where

$$\alpha = (Z - 2) / 3. \quad (17)$$

This implies

$$F(q^2) = \left[1 - \frac{\alpha}{2(2+3\alpha)} q^2 a^2 \right] e^{-a^2 q^2 / 4}. \quad (18)$$

Best fits to the data out to the diffraction minimum are given by $a = 1.64$ F ($F = 10^{-13}$ cm). Beyond the diffraction minimum, the best fit is given by a

slightly larger value of the oscillator parameter ($a = 1.68 \text{ F}$). In the region of the diffraction minimum the Born approximation (one-photon exchange) predicts zero. This is inconsistent with the data; however, it is well-known that a full phase-shift analysis¹⁶ predicts a minimum and not a zero. Because we need a closed form for the carbon elastic form factor we will use Eq. (18) as follows:

$$a = 1.64 \text{ F}, \quad q^2 \leq 3.2 \text{ F}^{-2};$$

$$a = 1.68 \text{ F}, \quad q^2 > 3.5 \text{ F}^{-2};$$

$$F^2(q^2) = 10^{-5}, \quad 3.2 < q^2 \leq 3.5 \text{ F}^{-2}.$$

Figure 2(a) shows a plot of the elastic form factor for carbon.

D. Excitation of Nuclear Levels

At present, the shell model is the basis for the most successful theoretical interpretations of the C^{12} level excitations. The ground state is composed of closed $1s_{1/2}$ and $1p_{3/2}$ shells. The interaction of the electron with the nucleus is viewed as an interaction with a single nucleon in a well-defined shell-model state which is then excited to one of the higher-lying unoccupied shells. de For-

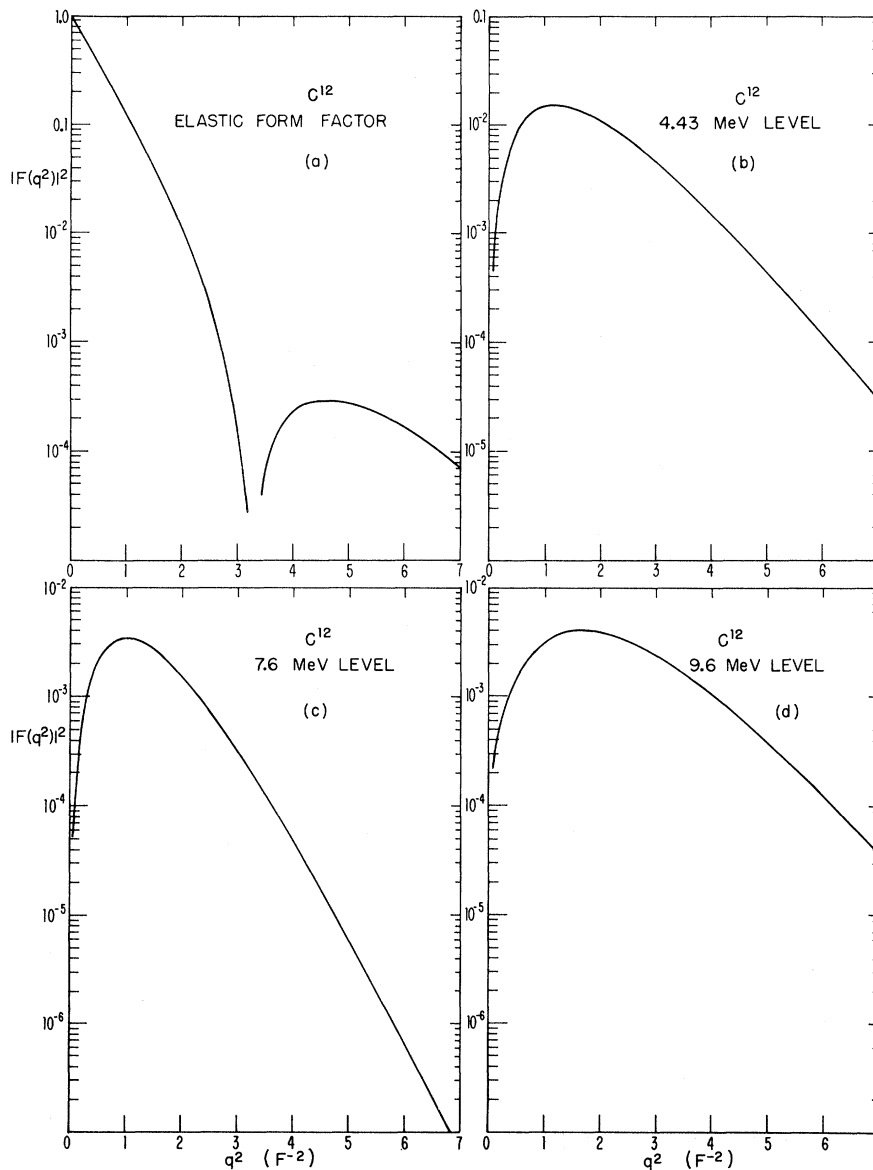


FIG. 2. Form factors for the carbon nucleus: (a) elastic scattering; (b) excitation of 4.43-MeV level; (c) excitation of 7.6-MeV level; (d) excitation of 9.6-MeV level.

est and Walecka⁴ give an excellent review of such calculations within the framework of Eq. (12) for the shell model as well as for other nuclear models.

A large number of data^{1-4, 17-30} are available for the excitation of levels in C^{12} . These data show levels or level complexes at excitation energies of 4.43, 7.76, 9.6, 15.11, 16, 19, and 22.8 MeV.

The last of these is generally referred to as the "giant resonance." These data were taken at incident electron energies less than one GeV and in general at angles much larger than those of this experiment.

Since the theoretical picture for the three lowest-lying levels seems to be confused,⁴ we have chosen to use empirical fits to the data. The expressions

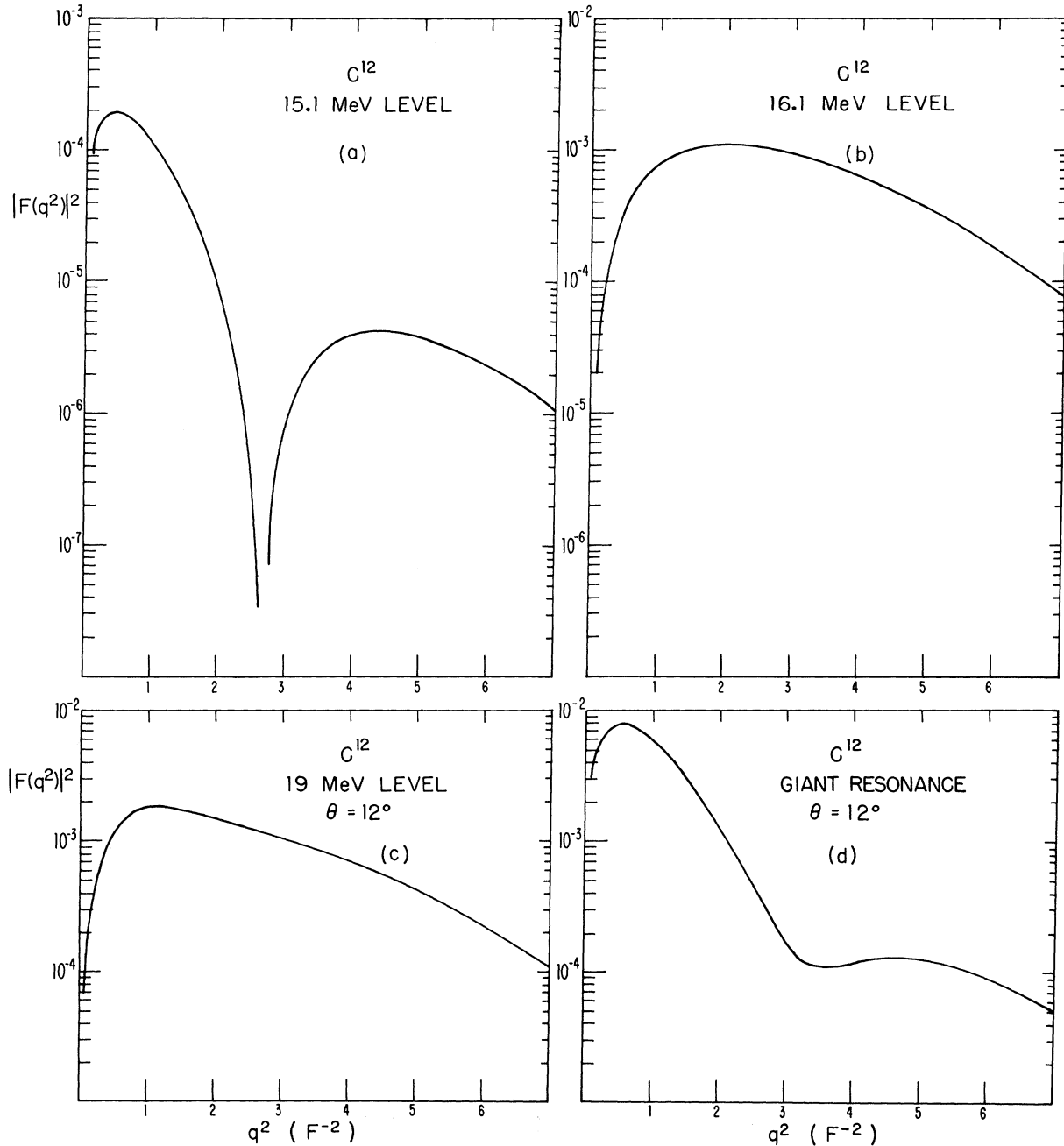


FIG. 3. Form factors for the carbon nucleus: (a) excitation of 15.1-MeV level; (b) excitation of 16.1-MeV level; (c) excitation of 19-MeV level; (d) excitation of the "giant resonance."

used are based on the shell-model predictions and are functions of only q^2 . They take the form of polynomials in q^2 times an exponential factor. These fits track the data better than the published theoretical fits. For the 4.43-MeV ($0^+ \rightarrow 2^+$), 7.76-MeV ($0^+ \rightarrow 0^+$), and 9.6-MeV ($0^+ \rightarrow 3^-$) levels, the data show no significant angular variation for fixed q^2 ; thus the fits, which assume dominance of w_2 over w_1 , are justified.

Donnelly, Walecka, Sick, and Hughes³¹ have reviewed the experimental and theoretical situation with respect to the remaining levels; we have relied exclusively on the shell-model interpretation of these authors.³² Figures 2(b) through 2(d) and 3(a) through 3(d) show the form factors used in the calculations for this experiment. The form factor plotted in these figures is defined by the equation

$$F^2(q^2) = \frac{d\sigma}{d\Omega} \left[\frac{Z^2 \sigma_M}{\eta} \right]^{-1}. \quad (19)$$

For purpose of these graphs the expressions for the 15.11-, 16-, 19-, and 22.8-MeV levels were evaluated for a laboratory scattering angle of 12° .

E. Scattering from a Free Nucleon

Prior to considering quasielastic scattering, we shall consider the elastic scattering from a free nucleon. For a free nucleon⁵

$$W_1 = q^2 \frac{M}{4} G_M^2(q^2) \delta(q \cdot P_3 - \frac{1}{2}q^2), \quad (20)$$

$$W_2 = \frac{G_E^2(q^2) + (q^2/4M)G_M^2(q^2)}{1 + (q^2/4M)} M^2 \delta(q \cdot P_3 - \frac{1}{2}q^2). \quad (21)$$

Inserting these expressions into Eq. (1) leads immediately to the Rosenbluth cross section

$$\frac{d\sigma_R}{d\Omega} = \frac{\sigma_M}{\eta} \left[\frac{G_E^2(q^2) + (q^2/4M^2)G_M^2(q^2)}{1 + (q^2/4M^2)} + 2 \tan^2 \frac{1}{2}\theta \frac{q^2}{4M} G_M^2(q) \right]. \quad (22)$$

Whenever the nucleon form factors are required we shall use the "dipole fit"³³

$$G_E^P = \frac{G_M^P}{2.79} = \frac{4M^2}{q^2} \frac{G_E^N}{(-1.91)} \\ = \frac{G_M^N}{(-1.91)} = \left[1 + \frac{q^2}{0.71 (\text{GeV}/c)^2} \right]^{-2}. \quad (23)$$

F. Quasielastic Scattering

Following the excitation of levels, the next region of energy loss to be considered is that of quasielastic scattering. The cross section in this region represents approximately scattering of the electron by a moving nucleon in the nucleus. A

study of this process gives a determination of the momentum distribution of the nucleons in the ground state of the nucleus. Several experiments have investigated this region of energy loss with incident electron energies of a few hundred MeV.^{22, 34-36} More recently, interest has arisen in the same experiment when the ejected proton in the final state is also detected. Such experiments have been performed by Amaldi *et al.*^{37, 38} at Frascati.

There has also been a great deal of theoretical interest in this process. Czyz³⁹ considered quasielastic scattering when $|\vec{q}| < k_f$, the Fermi momentum. He used the oscillator well model of the C¹² nucleus and obtained fair agreement with the data of Leiss and Taylor³⁴ on the large energy loss side of the quasielastic peak when the nucleon mass was replaced by an effective nucleon mass, $M^* < M$ to account for the binding energy of the nucleus. Henry^{40, 41} considered scattering from a Fermi model of the nucleus when $|\vec{q}| > 2k_f$ where the Pauli principle is no longer important in inhibiting the process. Moniz⁸ has considered all regions of \vec{q} for both the Fermi model and the oscillator well model. The Fermi model seems to give better agreement with the data of Leiss and Taylor³⁴ and Zimmerman³⁶ than the oscillator model. Other treatments of quasielastic scattering have been given by de Forest,⁴² Małeckı and Picchi,⁴³ Løvseth,⁴⁴ and Donnelly.⁴⁵ In addition to these calculations, several authors^{6, 46} have considered the effects of two-body nucleon correlations on the very high-energy loss tail of the quasielastic peak.

We now summarize the Moniz and Henry calculations since they will be used later to fit the data. Moniz divides his theory into two natural regions, $Q \equiv |\vec{q}|/k_F \leq 2$ and $Q > 2$, and makes different assumptions and approximations in each region. When $Q \leq 2$ the recoiling nucleon is not necessarily outside the Fermi sea; thus in this case the Pauli principle is important. Also when $Q \leq 2$ an effective nucleon mass is introduced as in the Czyz theory. For small energy loss the same effective mass is used for the recoiling nucleons since they still experience the nuclear potential. When $Q > 2$, the free nucleon mass is used and the effect of nuclear binding is included by shifting the quasielastic peak to higher-energy loss values by an average binding energy (~ 35 MeV). Throughout, Moniz considers only one-photon exchange. When $Q \leq 2$, nonrelativistic kinematics is assumed for both the target and recoil nucleon. When $Q > 2$, relativistic kinematics is assumed for the recoil particle.

Figures 4(a) and 4(b) show the doubly differential cross section predicted by Moniz at 1.5 GeV,

12° and 4.0 GeV, 18°. The first of these cases has $Q < 2$ and the latter has $Q > 2$.

Henry considers only the case of $Q > 2$ and assumes that the velocity of the initial nucleon is negligible compared to unity. In this approximation a remarkably simple result is obtained.

$$W_1 = \frac{3\epsilon_0 M_T}{4\epsilon_i \Delta\epsilon_f A^2} \frac{8}{q_0^2} \left[1 - \left(\frac{\epsilon_f - \epsilon_0}{\Delta\epsilon_f} \right)^2 \right] T_1(q_0^2), \quad (24)$$

and

$$W_2 = \frac{3\epsilon_0 M_T}{4\epsilon_i \Delta\epsilon_f A^2} \frac{2}{M^2} \left[1 - \left(\frac{\epsilon_f - \epsilon_0}{\Delta\epsilon_f} \right)^2 \right] T_2(q_0^2), \quad (25)$$

where

$$T_1(q^2) = \frac{1}{2} q^2 [Z G_M^{P^2}(q^2) + N G_M^{N^2}(q^2)], \quad (26)$$

and

$$T_2(q^2) = \frac{2M^2}{1 + q^2/4M^2} \left\{ Z \left[G_E^{P^2}(q^2) + \frac{q^2}{4M^2} G_M^{P^2}(q^2) \right] + N \left[G_E^{N^2}(q^2) + \frac{q^2}{4M^2} G_M^{N^2}(q^2) \right] \right\}. \quad (27)$$

Here

$$\epsilon_0 = \frac{\epsilon_i}{1 + (2\epsilon_i/M) \sin^2 \frac{1}{2} \theta}, \quad (28)$$

$$q_0^2 = 4\epsilon_i \epsilon_0 \sin^2 \frac{1}{2} \theta, \quad (29)$$

and

$$\Delta\epsilon_f = \frac{\epsilon_0^2 k_F}{\epsilon_i} (k_F^2 + M^2)^{-1/2} \sin \theta \left[1 + \left(1 + \frac{\epsilon_i}{M} \right)^2 \tan^2 \frac{1}{2} \theta \right]^{1/2}. \quad (30)$$

When expressed as a doubly differential cross section the simplicity of the above formulas is even more apparent. Equations (1) and (22) give

$$\frac{d^2\sigma}{d\Omega_f d\epsilon_f} = \frac{3}{4\Delta\epsilon_f} \left[1 - \left(\frac{\epsilon_f - \epsilon_0}{\Delta\epsilon_f} \right)^2 \right] \left[Z \left(\frac{d\sigma_R}{d\Omega} \right)_P + N \left(\frac{d\sigma_R}{d\Omega} \right)_N \right]. \quad (31)$$

Thus, the outgoing momentum spectrum, in Henry's calculation, is parabolic and is centered about the energy corresponding to scattering from a stationary nucleon. The parabolic function is normalized so that

$$\int \frac{d^2\sigma}{d\Omega_f d\epsilon_f} d\epsilon_f = Z \left(\frac{d\sigma_R}{d\Omega} \right)_P + N \left(\frac{d\sigma_R}{d\Omega} \right)_N. \quad (32)$$

Henry's prediction for 4.0 GeV, 18° is plotted alongside Moniz's prediction in Fig. 4(b). Henry in collaboration with Freiberg has extended this approach to the $Q \leq 2$ region with results in essential agreement with Moniz.⁴⁷

It is useful to consider Henry's approach when the recoiling nucleon has a mass M_f different from the nucleon mass. Following Henry's method as

described in Refs. 40 and 41, we integrate over initial nucleon momenta and angles with the kinematics now described by

$$\epsilon_f = \frac{\epsilon_i(1 - v_T \cos \xi_1) - (M_f^2 - M^2)/2M_T \gamma_T}{1 - v_T \cos \xi_2 + (2\epsilon_i/M_T \gamma_T) \sin^2 \frac{1}{2} \theta}, \quad (33)$$

where

$$\gamma_T = (1 - v_T^2)^{-1/2}, \quad (34)$$

$$\cos \xi_1 = \vec{P}_T \cdot \vec{p}_i / |\vec{P}_T| |\vec{p}_i|, \quad (35)$$

and

$$\cos \xi_2 = \vec{P}_T \cdot \vec{p}_f / |\vec{P}_T| |\vec{p}_f|. \quad (36)$$

When the final nucleon is considered to be a discrete higher-mass state, Eq. (31) still gives the correct cross section, but now

$$\epsilon_0 = \frac{\epsilon_i - (M_f^2 - M^2)/2M}{1 + (2\epsilon_i/M) \sin^2 \frac{1}{2} \theta}, \quad (37)$$

and

$$\Delta\epsilon_f(\epsilon_i, \epsilon_0, \theta) = \frac{\epsilon_i k_F (k_F^2 + M^2)^{-1/2}}{1 + (2\epsilon_i/M) \sin^2 \frac{1}{2} \theta} \times \left[\left(\cos \theta - \frac{\epsilon_0}{\epsilon_i} \right)^2 + \sin^2 \theta \right]^{1/2}. \quad (38)$$

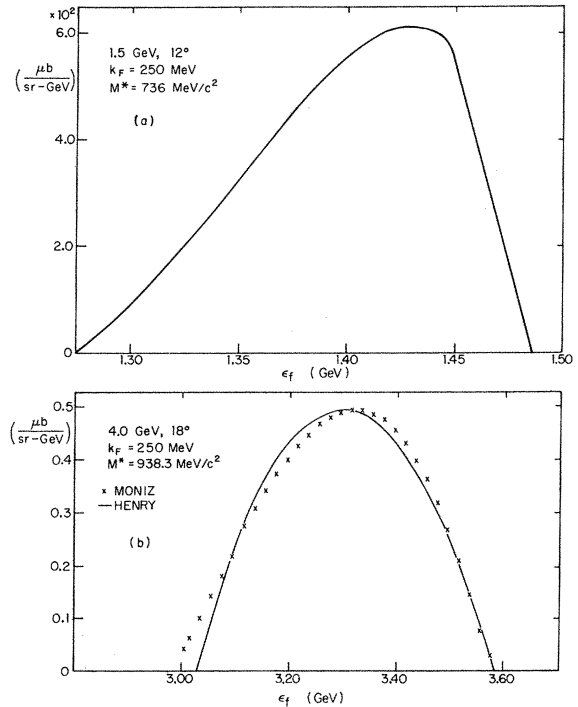


FIG. 4. The doubly differential cross section for quasi-elastic scattering from carbon predicted by the Fermi model of Moniz. Part (a) is for an incident energy of 1.5 GeV and a lab scattering angle of 12°. Part (b) is for an incident energy of 4.0 GeV and a scattering angle of 18°. Also shown in part (b) is the cross section calculated using the Fermi model of Henry.

Equation (38) reduces to Eq. (30) when $M_f = M$.

We can now determine the cross section for scattering from the nucleus when the final mass spectrum is a continuum, e.g., N_{33}^* production. Following Henry, we assume that the target nucleon velocity is much less than the velocity of light. We may then write

$$\frac{d^2\sigma}{d\Omega_f d\epsilon_f} = \int d\epsilon_0 \frac{d^2\sigma}{d\Omega d\epsilon_0}(\epsilon_i, \epsilon_0, \theta) \frac{3}{4\Delta\epsilon_f} \left[1 - \left(\frac{\epsilon_f - \epsilon_0}{\Delta\epsilon_f} \right)^2 \right], \quad (39)$$

where we have utilized Eqs. (31) and (38) plus the $v_T \ll 1$ assumption in order to rewrite Eq. (11) of Ref. 40. Notice that in all of the above expressions the cross section vanishes when $|(\epsilon_f - \epsilon_0)/\Delta\epsilon_f| > 1$. The cross section under the integral sign in Eq. (39) is the stationary electron-nucleon scattering cross section.

G. Nonresonant Pion Electroproduction

Czyz and Walecka⁴⁸ have considered pion electroproduction from $Z=N$, spin-zero nuclei. They employed the Fermi model of the nucleus and used the pion electroproduction amplitude of Fubini, Nambu, and Wataghin.⁴⁹ Keeping only the S -wave production, production proceeding through magnetic dipole excitation of $N_{33}^*(1236)$, and assuming only low-energy pions are produced, they arrived at expressions for the threshold behavior. The range of applicability of their results is stated to be about 30 or 40 MeV above the one-pion threshold. These results are summarized in power laws for the threshold behavior. When $|\vec{q}| < 2k_F$, π^0 coherent production dominates for several MeV above meson threshold and rises as $\lambda^{3/2}$ where

$$\lambda = (\epsilon_i - \epsilon_f - m_\pi)/m_\pi. \quad (40)$$

As the energy loss becomes greater the S -wave incoherent production begins to dominate and rises as $\lambda^{5/2}$. The interference between S -wave and resonant production, as well as the resonant production itself, rises as $\lambda^{7/2}$.

When $|\vec{q}| > 2k_F$ the incoherent processes remain zero until

$$\lambda \approx \frac{|\vec{q}|}{2M^*m_\pi} (|\vec{q}| - 2k_F); \quad (41)$$

thus, in this case, the threshold behavior is determined solely by the $\lambda^{3/2}$ characteristic of the π^0 coherent production.

H. Resonant Pion Electroproduction

Dufner and Tsai⁵⁰ have parametrized the data for $e + p \rightarrow e + N_{33}^*$ in the momentum transfer range $0.1 < q^2 < 2.33$ (GeV/c)². They use a simple isobar mod-

el which assumes dominance of the M_1 transition, and their basic result is a phenomenological fit to the γNN^* form factor expressed in terms of the C_3 coupling of Gourdin and Salin.^{51, 52} The result is given by

$$\frac{d^2\sigma}{d\Omega_f d\epsilon_f} = \frac{r_0^2 m_e^2}{q^2} \frac{\epsilon_f}{\epsilon_i} [\omega^2 + q^2 + (\epsilon_i + \epsilon_f)^2] \left(\frac{M}{M_f} \right)^2 \times \frac{\omega + M + M_f}{3M_f} \frac{C_3^2(q^2)}{\pi} \frac{2\Gamma M_f M_{33}}{(M_f^2 - M_{33}^2)^2 + \Gamma^2 M_{33}^2}, \quad (42)$$

where

$$[C_3(q^2)M]^2 = (2.05)^2 e^{-6.3\sqrt{q^2}} (1 + 9\sqrt{q^2}). \quad (43)$$

The resonance factor is the relativistic Breit-Wigner line shape of Jackson⁵³ with

$$\Gamma = \Gamma_0 \left(\frac{P^*}{P_R^*} \right)^{2l+1} \frac{am_\pi^2 + P_R^{*2}}{am_\pi^2 + P^{*2}}; \quad (44)$$

$$P^{*2}(M_f) = \left(\frac{M_f^2 - M^2 + m_\pi^2}{2M_f} \right)^2 - m_\pi^2; \quad (45)$$

and

$$P_R^* = P^*(M_{33}).$$

For the N_{33}^* we have

$$\Gamma_0 = \Gamma_{33} = 120 \text{ MeV}, \\ a = 1.384,$$

and

$$l = 1.$$

Because of the difficulty in subtracting the non-resonant background from the data, Dufner and Tsai suggest that Eq. (42) may be good to 10–15% at the N_{33}^* peak. Simple isospin arguments indicate that one should see as much N_{33}^* production from neutrons as from protons.

We obtain an expression for the excitation of the $N_{13}^*(1525)$ by using phase space modified by the relativistic line shape of Jackson. In this case we take $l=2$ and

$$\Gamma = \Gamma_0 (P^*/P_R^*)^{2l+1}. \quad (46)$$

For both cases, it is necessary to integrate the expressions for initially stationary nucleons over nucleon velocities and angles according to Eq. (39).

Moniz also calculates the cross section in the region of the N_{33}^* , treating the resonance as a discrete final state. Thus, his distribution for ϵ_f is due only to motion of the nucleons in the nucleus. His result may, therefore, be considered to be similar to Eq. (31) with ϵ_0 and $\Delta\epsilon_f$ given by Eqs. (37) and (38).

For this reason we have not chosen to fit the data to the Moniz spectrum in this region although

a comparison will be made. It should also be noted that because the recoil nucleon is now an N^* the Pauli principle is not considered in these calculations. However, the Pauli principle may inhibit the decay of the N^* in the nucleus.

III. RADIATIVE CORRECTIONS

As will be seen in Sec. VI our procedure is to radiatively correct the theory in order to make a direct comparison with the data rather than to attempt to unfold the data. We have used the results of Mo and Tsai⁵⁴ (MT) in order to make corrections for target bremsstrahlung and internal radiation. For discrete states the area under the peak is given by

$$\left(\frac{d\sigma}{d\Omega}\right)_{\text{measured}} = \left(\frac{d\sigma}{d\Omega}\right)_{\text{theory}} e^{\delta + \delta_t} \quad (47)$$

for a specified small maximum energy lost due to radiation. δ_t accounts for target bremsstrahlung and δ accounts for internal bremsstrahlung. For δ we have used the expression of Tsai as quoted by MT. We have included the terms in Z^2 .

In calculating the radiative tail from discrete states we have used a generalized form of Eq. (A16) of MT. The effects of internal bremsstrahlung are included in this approach by adding an "equivalent radiator" before and after scattering whose thickness is

$$t_r = \frac{1}{b} \frac{\alpha}{\pi} \left(\ln \frac{q^2}{m_e^2} - 1 \right). \quad (48)$$

Here b is a number whose value is close to $\frac{4}{3}$; the exact expression is given by MT. Equation (IV.1) of MT was used to correct the continuum (quasi-elastic scattering and meson production). This calculation incorporates both the strip and peaking approximations.

IV. APPARATUS

The apparatus used in this experiment is essentially the same as that employed in the repeat of the wide-angle electron pair experiment⁵⁵ and in the measurements on asymmetric electron pairs.⁵⁶ The spectrometer system consisted of two mirror-image spectrometer arms. Each arm contained a half quadrupole magnet, a number of scintillation counters, a threshold gas Čerenkov counter, and a shower counter. Hodoscope counters were used to divide the acceptance into six horizontal angle bins and five momentum bins. The experiment was on line to an SDS 92 computer which was in turn in communication with an IBM 360/50. Shower counter pulse heights were recorded along with the status of all scintillation counters and many low-order coincidences. The two arms were used to make independent measurements of the electron scattering cross sections. Figure 5 shows a plan view of one of the arms. The carbon target used was 1.091 g/cm² thick. It was located inside a vacuum chamber at the pivot of the spectrometer system. Table II summarizes the points at which data were taken and the spectrometer arm that was used in the measurements.

V. DATA REDUCTION AND CORRECTIONS

The data were corrected for dead time in the electronics ($\sim+2.5\%$), random coincidences ($\sim-2\%$), pion contamination due to knock on electrons ($\sim-3\%$), and the empty target rate ($<1\%$). A correction of -4.5% was applied to part of the data because of radiative losses in the unscattered beam. Due to bremsstrahlung in the target and beam pipe windows, some of the electrons in the beam lost energy and were swept out of the acceptance of the Faraday cup by the part of the beam

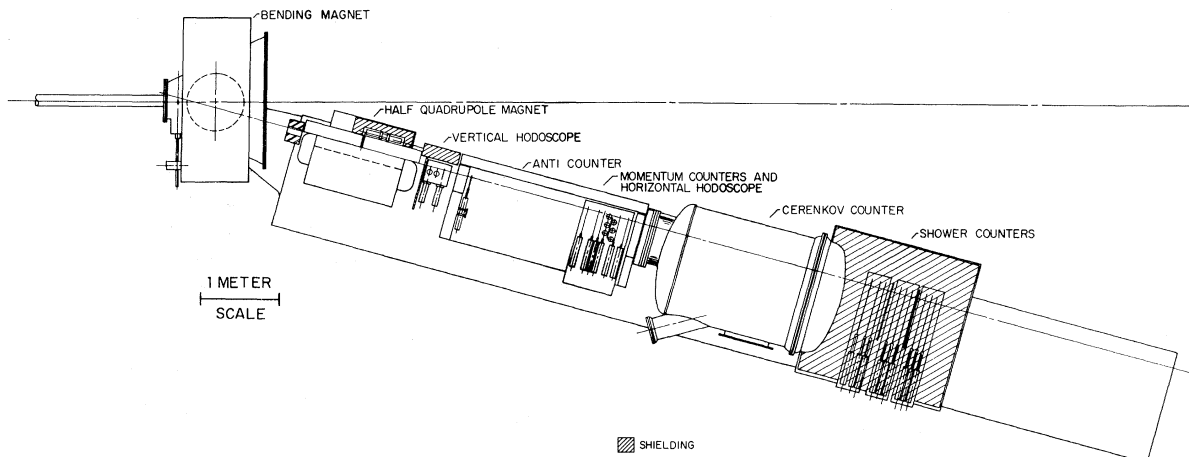


FIG. 5. Schematic diagram of the right arm showing the relative location of the magnets and counters.

TABLE II. Points at which data were taken. The energy and angle are the nominal values.

Incident energy (GeV)	Angle (deg)	Elastic q^2 (GeV/c) ²	q^2 (F^{-2})	Spectrometer
1.0	8.5	0.022	0.565	Right
1.5	8.5	0.049	1.26	Left
1.5	12.0	0.098	2.52	Right
2.25	8.5	0.111	2.85	Right
3.0	8.5	0.197	5.06	Left
3.0	12.0	0.391	10.0	Right
3.0	12.0	0.391	10.0	Left
3.0	18.0	0.870	22.3	Right
4.0	12.0	0.694	17.8	Left
4.0	18.0	1.539	39.5	Right

transport system following the target. This transport system was only used during some of the runs. In addition, the raw counting rates on some of the points were adjusted by as much as -6.3% by event selection criteria based on the hodoscope patterns.

The corrected rates were converted to cross sections averaged over the apparatus acceptance by using the expression

$$\frac{d^2\sigma}{d\Omega dp} = \frac{\text{corrected rate}}{N_I N_T \int dp d\Omega A(p, \theta, \varphi)}. \quad (49)$$

Here N_I and N_T are the number of incident particles/sec and the number of target nuclei/cm², respectively. N_I was measured with a Faraday cup whose calibration was known to an accuracy of $\pm 0.5\%$. The phase-space integral, $\int dp d\Omega A(p, \theta, \varphi)$, for the apparatus was determined by a Monte Carlo program to a precision of better than $\pm 1\%$. The doubly differential cross sections resulting from this procedure are the desired cross sections integrated over the acceptance function of the apparatus. Spectra made up from a composite of such cross sections are shown in Figs. 6 and 7. Figure 8 shows some spectra from the previously reported experiment.⁹ The error bars represent a quadrature combination of statistical errors and random errors associated with the various correc-

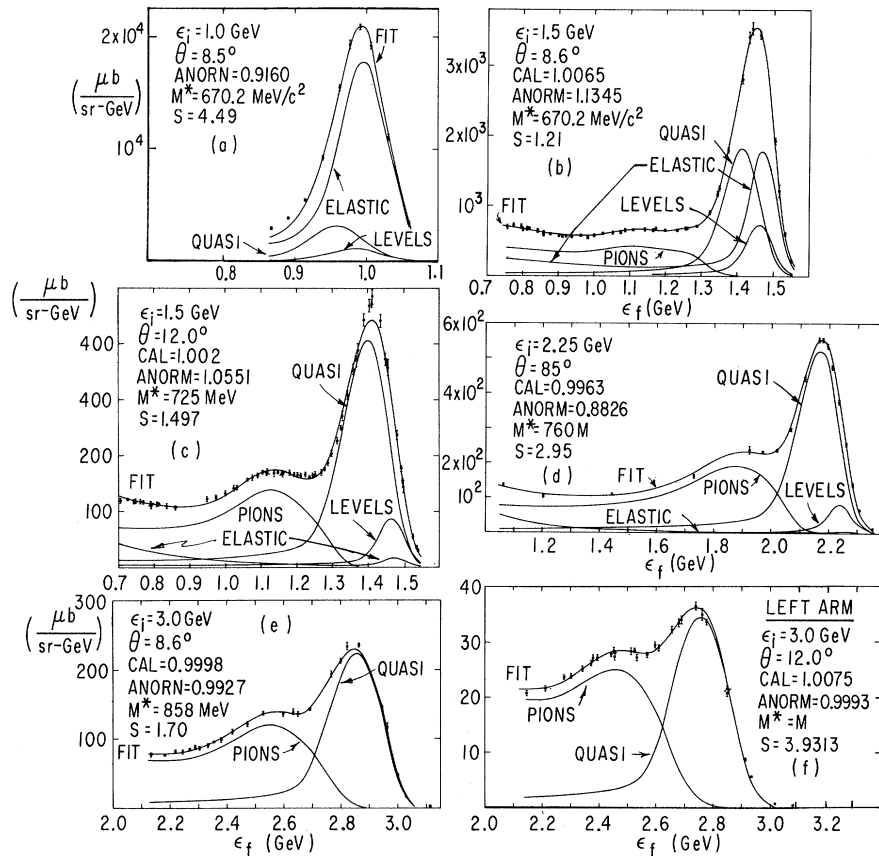


FIG. 6. Experimental differential cross section for scattering of electrons from carbon. The figures on each graph show the nominal incident energy and the nominal scattering angle. The curves show the fit to the data and the various components of the fit. The data shown in this figure were the new data.

tions. The over-all systematic error in the normalization is estimated to be $\pm 5\%$.

VI. COMPARISON OF THEORY AND EXPERIMENT

A. Procedure

The comparison of data and theory was carried out by means of a FORTRAN program which calculated the expected counting rate by folding the experimental resolution function with the radiatively corrected theory. These integrals were performed numerically using the acceptance functions determined by the Monte Carlo calculation and the smearing effect of multiple Coulomb scattering calculated using the theory of Moliere as reported by Scott.⁵⁷ Figure 9 shows the effect of multiple scattering on the momentum acceptance function for a single momentum bin. The theoretical spectrum was parametrized, and fitting routines chose the values of the parameters so as to minimize χ^2 .

The parameters of the fit included an over-all normalization of the theory (ANORM); the momentum calibration relative to the expected value (CAL); and several parameters associated with the pion spectrum. The relative normalizations of

the levels, elastic peak, and quasielastic peak were not varied. For many of the data points the elastic and levels cross sections are negligible. At these points ANORM gives a direct measure of the success of the Moniz prediction for the quasielastic scattering.

χ^2 was sensitive to the central value of the spectrometer momentum acceptance when the quasielastic peak was well resolved from the pion contribution. At these points the spectrometer energy calibration was allowed to vary in the fitting procedure, and in all such cases the value obtained for the calibration was within 0.5% of the expected value. When the quasielastic peak was poorly resolved from the pion background (generally for $Q > 2$ points) the momentum calibration was fixed at the value determined from elastic scattering and the theory was displaced ~ 35 MeV in order to account for the average effect of nucleon binding.

We relied upon the 1.0 GeV, 8.5° data, which are dominated by elastic scattering, to give us an accurate determination of the shape of the apparatus resolution function. For this point the data were fit with the rms of the multiple scattering distribu-

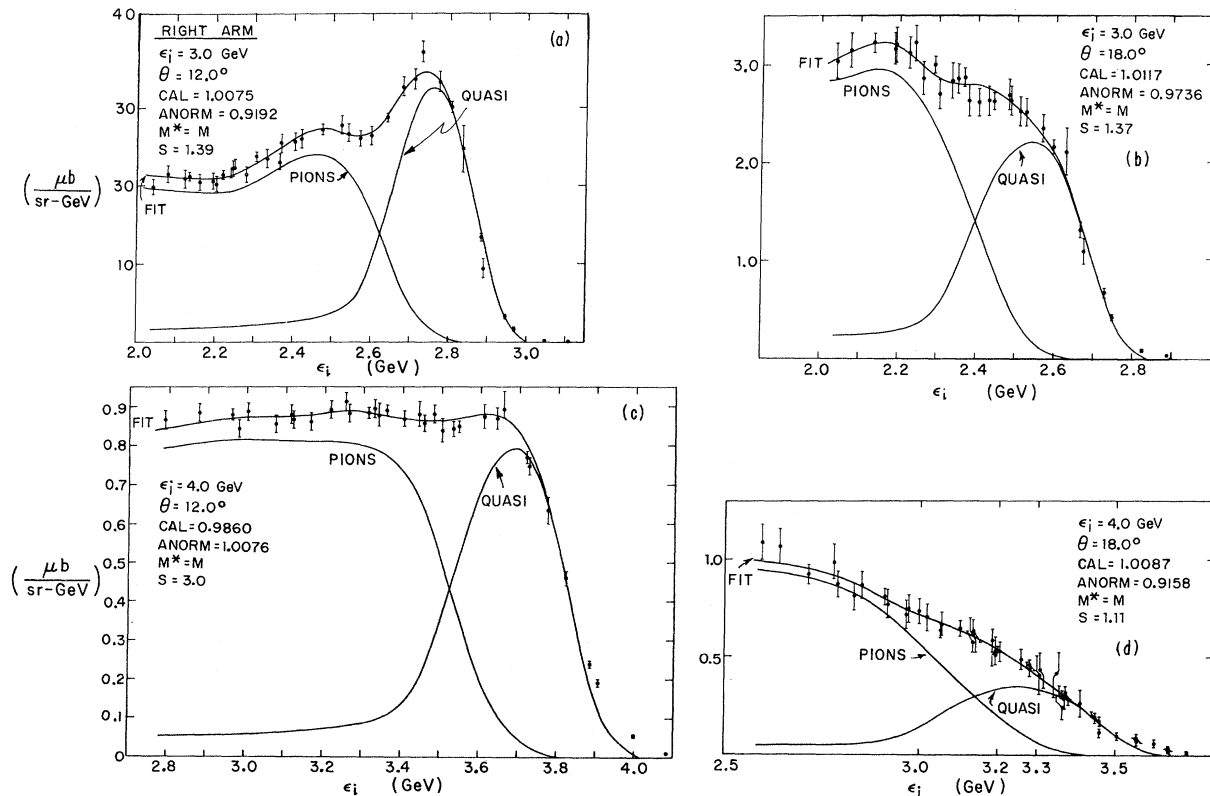


FIG. 7. Experimental differential cross sections for scattering of electrons from carbon. The figures on each graph show the nominal incident energy and the nominal scattering angle. The curves show the fit to the data and the various components of the fit. The data shown in this figure were the new data.

tion as a parameter. Figure 6(a) shows that in the region of the elastic peak the fit is very good. In order to obtain the best fit, the multiple scattering rms was increased by 9.3% of its predicted value. In fitting the remainder of the data, the resolution was fixed at this value.

A flexible expression for the pion spectrum was built from four separate contributions. The $N^*(1236)$ and $N^*(1525)$ contributions were calculated from Eq. (39). To this was added three-body phase space integrated over initial nucleon velocities according to Eq. (39). The threshold behavior for nonresonant production was joined onto phase space by allowing the cross section to rise as the sum of three independent terms ($\lambda^{3/2}$, $\lambda^{5/2}$, $\lambda^{7/2}$) up to a cutoff above threshold (CUT1) MeV. For higher-energy losses the threshold behavior was turned off linearly so that it fell to zero at a distance (CUT1 + CUT2) MeV above threshold. In this way a smooth expression for the nonresonant production was obtained which adequately reflects our knowledge in the threshold region and which is determined by phase space in the deeper inelastic region. The fitting parameters in the meson

production region were CUT1, CUT2, and six amplitudes, one each for the two resonances, the three threshold terms, and phase space. The resulting pion spectrum is a flexible phenomenological expression which allows good fits to the data. We do not necessarily expect to resolve the resonant behavior from the nonresonant in this way. However, the total pion cross section should be determined accurately by this method. More exactly, the excess in cross section over the Moniz calculation of the quasielastic scattering should be determined accurately. Thus, if there is a significant deviation from this calculation due to nucleon correlations this would appear as additional cross section in the meson production region of the fit. The fitting procedure is therefore a consistent-technique for subtracting the elastic, levels, and quasielastic contributions from the experimental spectra. At the same time, we obtain information regarding the normalization and shape of the quasielastic spectrum.

In applying the quasielastic theory we have followed Moniz's suggestion regarding M^* .⁸ For $Q < 1$, we choose $M^* = M/1.4$, the nuclear matter val-

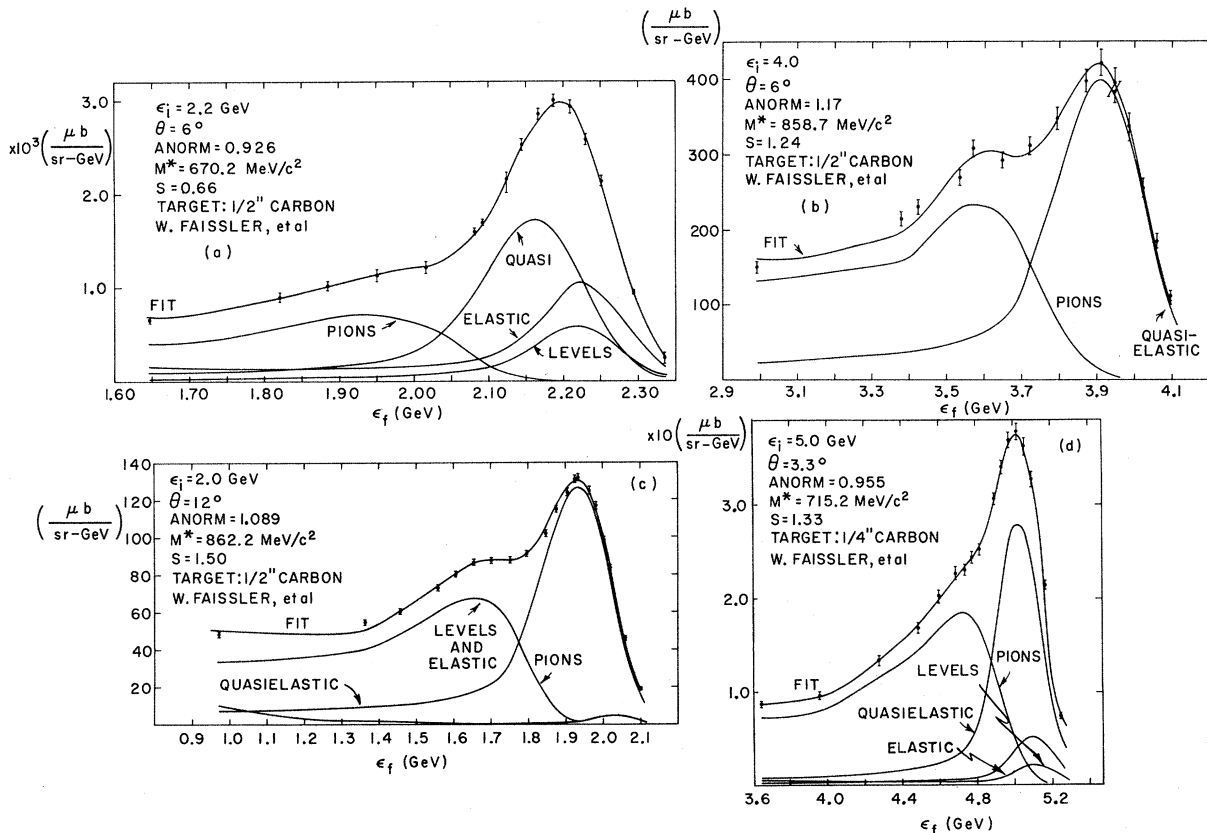


FIG. 8. Experimental differential cross sections for scattering of electrons from carbon. The figures on each graph show the nominal incident energy and the nominal scattering angle. The curves show the fit to the data and the various components of the fit. The data shown in this figure were from the previously reported experiment of Faissler *et al.*

ue. For $Q > 2$, $M^* = M$. Between $Q = 1$ and $Q = 2M^*$ is allowed to rise linearly with Q . For the C^{12} Fermi momentum we used 250 MeV.

The data of Faissler, Pipkin, and Stanfield⁹ were reanalyzed and fit by a similar procedure. This provided a more accurate treatment of multiple scattering, radiative corrections, and the quasielastic theory than was used previously.

B. Data and Results of Fitting Procedure

The data and the components of the fits are graphed in Figs. 6–8 with the important parameters as labels. The curve labeled PIONS is the sum of all the components of the fit in the meson production region.

In general the fits track the data rather well over most of the spectrum. However, in almost every case the value of χ^2 is larger than expected by a significant amount. In the figures we quote a quantitative measure of this in terms of the value of S .

$$S = [\chi^2 / (N - 1)]^{1/2}, \quad (50)$$

where N is the number of degrees of freedom for the fit. Most of the χ^2 comes from the low-energy loss (large ϵ_f) region where the shape of the predicted spectrum is very insensitive to variations in the fitting parameters.

C. Quasielastic Scattering

Table III gives a summary of the fits for the quasielastic peak. The errors on ANORM are an estimate of the variation in systematic errors from point to point due to corrections such as hodoscope normality, surveying variations, and radiative corrections. The statistical error is negligible. The results of this experiment are consistent with the normalization determined by the dipole fit to the nucleon form factors and the Fermi model of Moniz. If the shape of the momentum spectrum had included a tail on the low-energy-loss side of the peak the agreement would have improved and χ^2 would have been considerably reduced. Determinations of the high-energy-loss side of the peak are confused by the pion threshold region. Early attempts to fit the spectra in the pion region with only phase space plus a resonance failed rather badly; an excess in the pion threshold region or on the high-energy-loss side of the quasielastic peak was required. The present treatment using the threshold polynomial provided a means by which to fit the curve and determine the excess. This excess can be attributed to a combination of a tail on the high-energy-loss side of the quasielastic peak and nonresonant pion production. We conclude that the Fermi model is qualita-

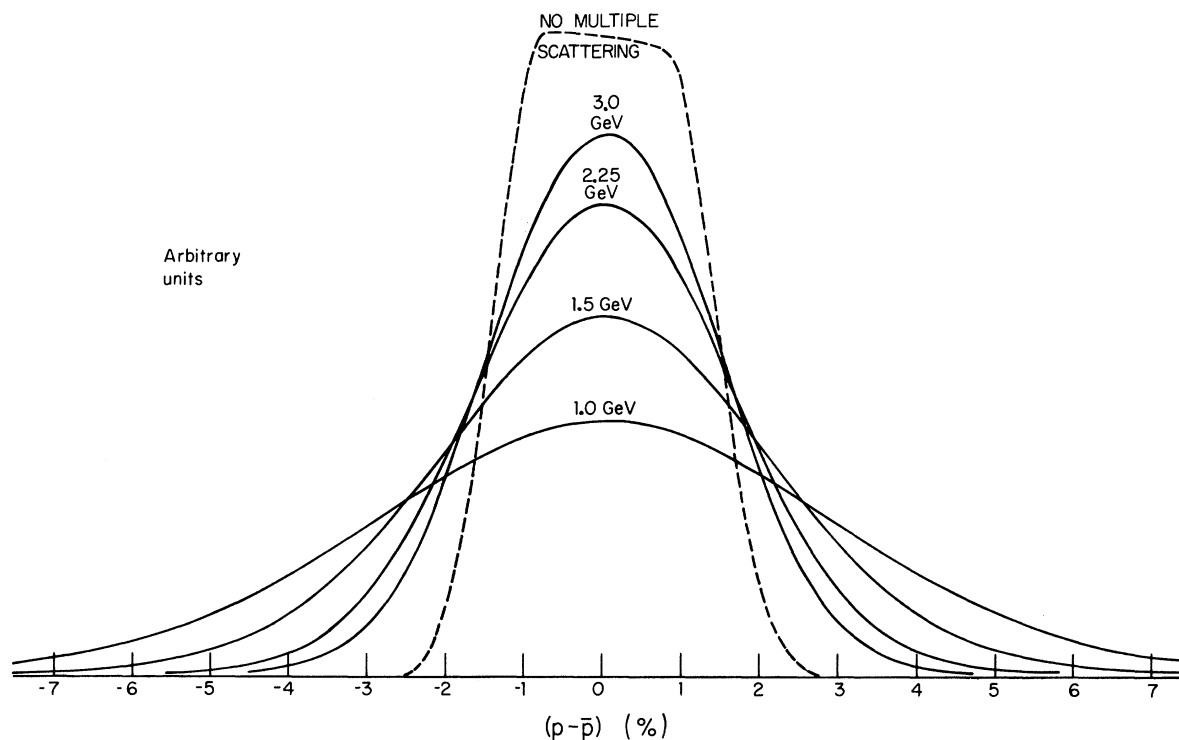


FIG. 9. The calculated shape of the acceptance function for a single momentum bin due to a combination of counter size and multiple scattering. The Moliere multiple-scattering theory was used in this calculation.

TABLE III. Summary of fits for the quasielastic peak.

ϵ_i (GeV)	θ_{ave} (deg)	CAL	M^* (MeV)	S	ANORM	Spectrometer
0.997	8.504	0.997	670.2	4.5	$0.916 \pm 5\%$	Right
1.486	8.575	1.007	670.2	1.2	1.135	Left
1.486	11.997	1.002	725.0	1.5	1.055	Right
2.250	8.515	0.996	760.0	2.9	0.883	Right
2.983	8.586	1.000	858.0	1.7	0.993	Left
2.983	12.060	1.008	M	3.9	1.000	Left
2.983	12.002	1.008	M	1.4	0.919	Right
2.983	17.953	1.012	M	1.4	0.974	Right
3.985	12.059	0.986	M	3.0	1.008	Left
3.985	17.951	1.009	M	1.1	0.916	Right
1.004	3.232	1.002	670.2	2.0	$1.101 \pm 10\%$	Faissler
4.018	3.287	0.995	680.9	1.0	0.952	Faissler
5.022	3.286	0.981	715.2	1.3	1.090	Faissler
5.022	3.287	0.979	715.2	1.4	0.962	Faissler
1.107	6.103	1.103	670.2	1.9	1.022	Faissler
2.217	6.111	0.990	670.2	0.7	0.926	Faissler
3.330	6.121	0.991	778.4	1.1	1.083	Faissler
4.018	6.120	0.993	858.7	1.2	1.174	Faissler
5.022	6.120	0.991	M	1.2	1.051	Faissler
1.117	12.106	0.998	670.2	2.0	1.138	Faissler
2.035	12.119	0.988	862.2	1.5	1.089	Faissler
5.022	12.112	0.933	670.2	1.5	0.988	Faissler

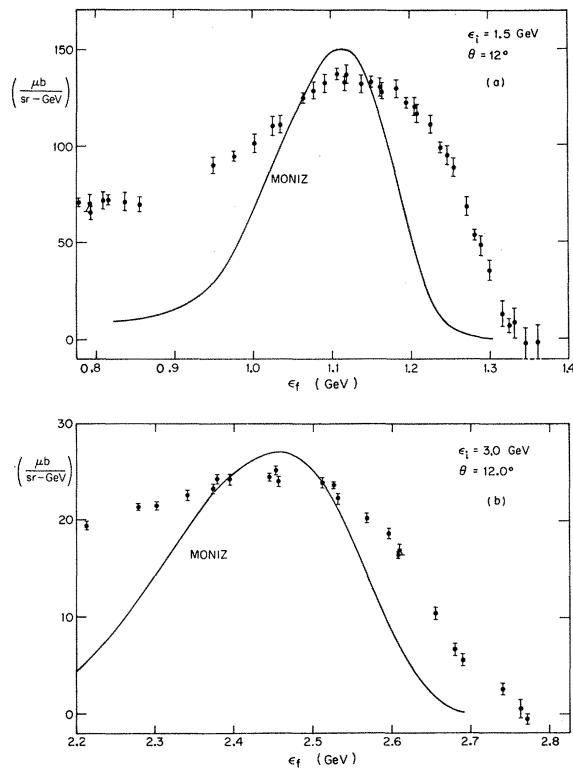


FIG. 10. A comparison between the measured differential cross section for the region of energy loss beyond the one-pion threshold and the pion electroproduction theory of Moniz.

tively correct in this region but that the distribution needs tails.

D. Pion Electroproduction

Figure 10 shows the N_{33}^* enhancement as determined by two of the data points. The data plotted are given by a direct subtraction of the sum of the quasielastic, levels, and elastic contributions from the data curves of Figs. 6 and 7. Also plotted in Fig. 10 is the prediction of Moniz for the N_{33}^* peak with $C_3(q^2)$ given by the phenomenological fit of Dufner and Tsai. In order to make this comparison, the theory has been integrated over the apparatus resolution and radiatively corrected according to the "strip approximation" of Mo and Tsai. It is obvious from the figure that the agreement is not good. There are several possible explanations for the disagreement. Moniz assumes that the N_{33}^* is a discrete state so that the spectrum is determined only by the Fermi motion of the nucleons. No nonresonant threshold behavior is included in the theory for this comparison. Finally, as was stated above if for any reason there is an excess in counting rate in the high-energy loss region of the quasielastic peak, this excess will appear in the threshold region of the pion spectrum.

The magnitude of the N_{33}^* peak was compared with the hydrogen data in the literature. Following Hand⁵⁸ the doubly differential electron scattering cross section is written

$$\frac{d^2\sigma}{d\Omega_f d\epsilon_f} = \Gamma_t(K, q^2, \epsilon_i) \sigma_t(K, q^2) + \Gamma_s(K, q^2, \epsilon_i) \sigma_s(K, q^2), \quad \frac{1}{\Gamma_t} \frac{d^2\sigma}{d\Omega_f d\epsilon_f}, \quad (54)$$

where

$$\Gamma_t = \frac{\alpha}{4\pi^2} \frac{K}{q^2} \frac{\epsilon_f}{\epsilon_i} \left[2 + \frac{\cot^2 \frac{1}{2}\theta}{1 + q_0^2/q^2} \right], \quad (52)$$

and

$$\Gamma_s = \frac{\alpha}{4\pi^2} \frac{K}{q^2} \frac{\epsilon_f}{\epsilon_i} \left[\frac{\cot^2 \frac{1}{2}\theta}{1 + q_0^2/q^2} \right]. \quad (53)$$

$\sigma_T(K, q^2)$ and $\sigma_s(K, q^2)$ are the total photoabsorption cross sections for transverse and scalar virtual photons, respectively. The data are quoted in terms of the ratio

which for small Γ_s is seen to approximate closely $\sigma_T(K, q^2)$. Table IV gives this ratio for the C^{12} data at $K = 345$ MeV, on the N_{33}^* peak. In Fig. 11 the C^{12} data are compared to twelve times the hydrogen data.⁵⁹⁻⁶⁴ The carbon numbers were obtained by reconstructing the pion spectrum from the parameters of the best fits to the data. The total uncertainty due to the method in which the radiative corrections were applied was estimated to be $\pm 5\%$; this is included in the errors quoted in Table IV.

The carbon N_{33}^* data are observed to have the same q^2 dependence as the hydrogen data while the magnitude is 15-20% lower than 12 times the hy-

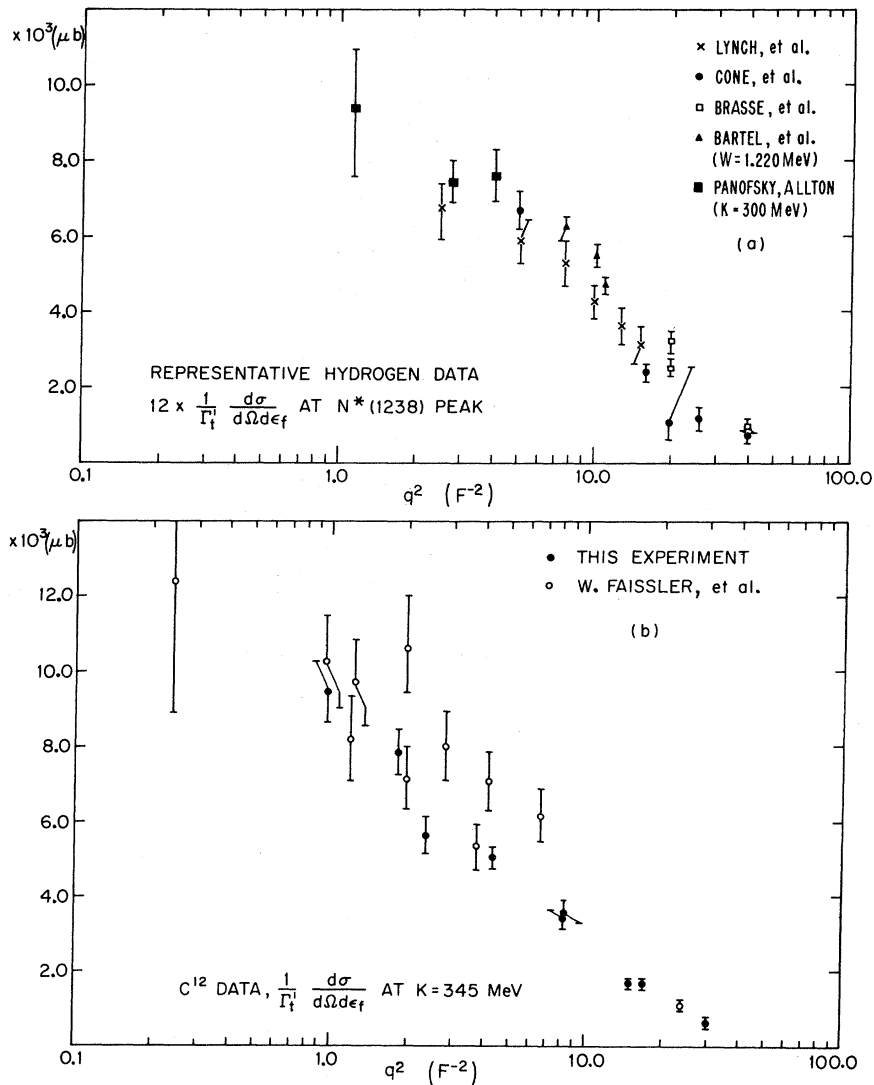


FIG. 11. A comparison between the cross section for pion electroproduction from carbon and the cross section for pion electroproduction from hydrogen.

drogen data. This difference is probably due to the Fermi motion smearing of the N_{33}^* peak. We conclude that coherent processes are not significantly present and that the N_{33}^* decay is not drastically inhibited in the nucleus.

E. Drell-Schwartz Sum Rule

Drell and Schwartz derived the following fixed-angle, fixed-incident-electron-energy sum rule^{65, 66}:

$$\int Z^2(W_2 + 2 \tan^2 \frac{1}{2} \theta W_1) d\epsilon_f = [G_E^P(q^2)]^2 \left\{ Z + Z(Z-1)f_2 + \frac{Zq^2}{2AM^2} + (2 \tan^2 \frac{1}{2} \theta + 1) \left[\frac{2}{3} \frac{Z}{AM} \langle T \rangle + \frac{q^2}{4M^2} (Z\mu_p^2 + N\mu_n^2) \right] \right\}. \quad (55)$$

Here f_2 is the form factor for the carbon nucleus which takes account of both elastic and inelastic scattering with excitation of nuclear levels. Equation (55) neglects the term which depends upon correlated scattering by nucleons in the nucleus. For carbon

$$Z(Z-1)f_2 = e^{-x}(30 - 16x + 8x^2/9), \quad (56)$$

where

$$x = \frac{1}{2}q^2a^2,$$

$$a = 1.637 \text{ F},$$

$$\langle T \rangle = 20 \text{ MeV}.$$

The experimental data can be used to derive the summed cross section

$$\frac{d\sigma_{\text{el}}}{d\Omega_f} = \int \frac{d\sigma}{d\Omega_f d\epsilon_f} d\epsilon_f, \quad (57)$$

where the integration is over all the processes which do not produce mesons: that is elastic scattering, nuclear level excitation and quasielastic scattering. The effective integrated W_2 is then calculated from the equation

$$\int W_2 d\epsilon_f = \left(\frac{d\sigma_{\text{el}}}{d\Omega_f} \right)_{\text{expt.}} \left[\frac{Z^2 \sigma_M}{\eta} \right]^{-1}. \quad (58)$$

Figure 12 shows a comparison of the Drell-Schwartz sum rule with the experimental value for the integrated W_2 . Figure 12 also shows the integrated W_2 calculated using the measured form factor for elastic scattering and level excitation and the quasielastic cross section of Moniz. The agreement between the different cross sections is good and indicates the accuracy of both theories in describing the over-all cross section.

TABLE IV. Meson electroproduction cross sections for C^{12} at $K = 345 \text{ MeV}$.

ϵ_i (GeV)	θ (deg)	q^2 (F ⁻²)	$\frac{d^2\sigma^a}{d\Omega_f d\epsilon_f}$ ($\mu\text{b}/\text{sr GeV}$)	$\frac{1}{\Gamma_t} \frac{d^2\sigma^a}{d\Omega_f d\epsilon_f}$ ($10^4 \mu\text{b}$)	$\frac{1}{\Gamma_t} \frac{d^2\sigma}{d\Omega_f d\epsilon_f}$ ($10^4 \mu\text{b}$)	Spectrometer
1.1	6.0	0.244	1355.	1.081	1.243 ± 0.363	Faessler
1.5	8.5	0.956	446.8	0.8455	0.946 ± 0.080	Left
1.1	12.0	0.960	201.1	0.8144	1.036 ± 0.125	Faessler
2.2	6.0	1.20	650.1	0.6250	0.818 ± 0.113	Faessler
4.0	3.3	1.24	2837.	0.7442	0.976 ± 0.113	Faessler
1.5	12.0	1.83	141.3	0.6742	0.782 ± 0.060	Right
5.0	3.3	1.97	2209.	0.6924	1.061 ± 0.120	Faessler
5.0	3.3	1.97	2039.	0.6395	0.713 ± 0.083	($\frac{1}{2}$ -in. C target) Faessler
2.25	8.5	2.36	198.8	0.5031	0.556 ± 0.047	($\frac{1}{4}$ -in. C target) Right
3.3	6.0	2.85	492.1	0.5922	0.798 ± 0.091	Faessler
2.0	12.0	3.75	69.34	0.4789	0.536 ± 0.061	Faessler
4.0	6.0	4.22	279.5	0.4870	0.706 ± 0.084	Faessler
3.0	8.5	4.36	123.4	0.4492	0.506 ± 0.038	Left
5.0	6.0	6.67	171.0	0.4140	0.620 ± 0.071	Faessler
3.0	12.0	8.23	24.70	0.2928	0.340 ± 0.025	Right
3.0	12.0	8.31	25.63	0.3091	0.358 ± 0.029	Left
4.0	12.0	14.98	7.730	0.1585	0.166 ± 0.013	Left
3.0	18.0	16.99	2.675	0.1449	0.165 ± 0.015	Right
5.0	12.0	24.00	2.884	0.0968	0.108 ± 0.013	Faessler
4.0	18.0	29.95	0.5873	0.0587	0.063 ± 0.008	Right

^aBefore radiative correction is applied to the resonant part.

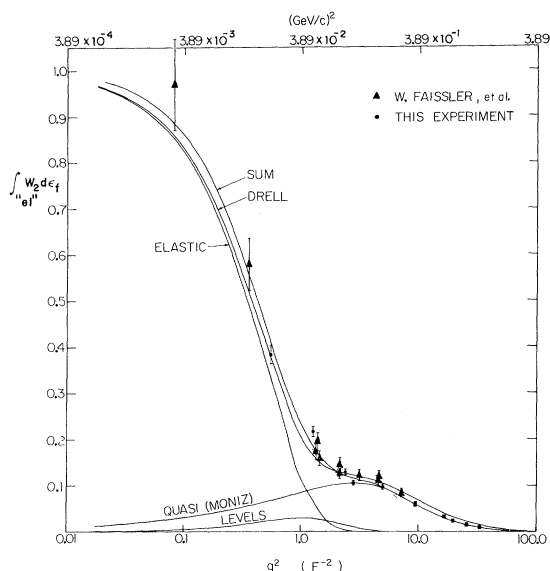


FIG. 12. Experimental and theoretical integrated form factors versus the four-momentum transfer squared. DRELL is an evaluation of the sum rule due to Drell and Schwartz, ELASTIC is the elastic scattering form factor, LEVELS is the sum of the form factors for nuclear level excitation, QUASI (MONIZ) is the form factor for quasi-elastic scattering calculated by the prescription of Moniz, SUM is the sum of ELASTIC, LEVELS, and QUASI. The experimental data are shown as points.

VII. CONCLUSIONS

The present experiment adds a large new body of data to that already existing for electron scat-

tering from carbon. Using the Cambridge Electron Accelerator we have obtained higher incident energies, momentum transfers, and energy losses than previously reported. We have studied in particular quasielastic scattering and pion electroproduction.

The Fermi model as formulated by Moniz gives a very successful description of the quasielastic scattering. The data suggest, however, that there are tails on the nucleon momentum distribution which are not accounted for by the theory. The pion electroproduction cross section in the region of the N_{33}^* is approximately equal to that expected for 12 independent nucleons. There is no large coherent production and the decay of the N_{33}^* in the nucleus does not appear to be significantly inhibited. The summed cross section for elastic scattering, level excitation, and quasielastic scattering is in agreement with that predicted by the Drell-Schwartz sum rule.

VIII. ACKNOWLEDGMENTS

We wish to acknowledge the support and encouragement of the director and staff of the Cambridge Electron Accelerator throughout the course of this experiment. We also wish to thank the staff of the Harvard Cyclotron Laboratory for their support. Other members of the group who contributed significantly to the success of the experiment are W. Cooper, A. M. Eisner, G. J. Feldman, N. Hicks, L. Litt, W. Lockeretz, V. Montana, J. K. Randolph, and J. Tenenbaum.

†Based in part on a thesis submitted by one of the authors (KCS) to Harvard University in partial fulfillment of the requirements for the Doctor of Philosophy in Physics. Work supported by the U. S. Atomic Energy Commission under Contract No. At(30-1) 2752.

*Present address: Harrison M. Randall Laboratory of Physics, the University of Michigan, Ann Arbor, Michigan 48104.

‡Work supported in part by National Science Foundation Graduate Traineeship.

§Present address: Physics Department, Northeastern University, Boston, Massachusetts 02136.

¹For a general review article on electron scattering see, R. Hofstadter, *Ann. Rev. Nucl. Sci.* **7**, 231 (1957).

²For a collection of reprints on electron scattering see, R. Hofstadter, in *Electron Scattering and Nuclear and Nucleon Structure*, edited by R. Hofstadter (W. A. Benjamin, Inc., New York, 1963).

³For a review article on inelastic electron scattering as a tool for exploring nuclear structure see, W. C. Barber, *Ann. Rev. Nucl. Sci.* **12**, 1 (1962).

⁴For a general review article on electron scattering

and nuclear structure see, T. de Forest, Jr., and J. D. Walecka, *Advan. Phys.* **15**, 1 (1966).

⁵S. D. Drell and J. D. Walecka, *Ann. Phys. (N.Y.)* **28**, 18 (1964).

⁶W. Czyz and K. Gottfried, *Ann. Phys. (N.Y.)* **21**, 47 (1963).

⁷J. D. Walecka, private communication.

⁸E. J. Moniz, *Phys. Rev.* **184**, 1154 (1969).

⁹W. Faissler, F. M. Pipkin, and K. C. Stanfield, *Phys. Rev. Letters* **19**, 1202 (1967).

¹⁰J. Fregeau, *Phys. Rev.* **104**, 225 (1956).

¹¹D. G. Ravenhall, *Rev. Mod. Phys.* **30**, 430 (1958).

¹²L. J. Tassie and F. C. Barker, *Phys. Rev.* **111**, 940 (1958).

¹³V. Meyer-Berkhout, K. W. Ford, and A. E. Green, *Ann. Phys. (N.Y.)* **8**, 119 (1959).

¹⁴H. F. Ehrenberg, R. Hofstadter, V. Meyer-Berkhout, D. G. Ravenhall, and S. Sobottka, *Phys. Rev.* **113**, 666 (1959).

¹⁵H. Cranell, *Phys. Rev.* **148**, 1107 (1966).

¹⁶D. R. Yennie, R. N. Wilson, and D. G. Ravenhall, *Phys. Rev.* **95**, 500 (1954).

- ¹⁷J. Fregeau, Phys. Rev. 104, 225 (1956) (4.43, 7.76, 9.6 MeV).
- ¹⁸H. F. Ehrenberg, R. Hofstadter, V. Meyer-Berkhout, R. G. Ravenhall, and S. E. Sobottka, Phys. Rev. 113, 666 (1959) (4.43 MeV).
- ¹⁹W. C. Barber, F. Berthold, G. Fricke, and F. E. Gud- den, Phys. Rev. 120, 2081 (1960) (15.1, 23 MeV).
- ²⁰B. Dudelzak and R. E. Taylor, J. Phys. Radium 22, 544 (1961) (15.1, 16 MeV).
- ²¹R. D. Edge and G. A. Peterson, Phys. Rev. 123, 2750 (1962) (15.1 MeV).
- ²²P. Boumin and G. R. Bishop, J. Phys. Radium 24, 974 (1963) (4.43, 16, 19.8 MeV).
- ²³J. Goldemberg and W. C. Barber, Phys. Rev. 134, B963 (1964) (18.1, 19.5, 24, 34 MeV).
- ²⁴F. Gudden, Phys. Letters 10, 313 (1964) (15.1 MeV).
- ²⁵J. Goldemberg, W. C. Barber, F. H. Lewis, Jr., and J. D. Walecka, Phys. Rev. 134, B1022 (1964) (15.1 MeV).
- ²⁶T. de Forest, Jr., J. D. Walecka, G. Vanpraet, and W. C. Barber, Phys. Letters 16, 311 (1965) (20.76, 21.34 MeV).
- ²⁷H. Crannell, H. A. Dahl, and F. H. Lewis, Jr., Phys. Rev. 155, 1062 (1967) (19.5 MeV).
- ²⁸G. R. Bishop, Phys. Rev. Letters 19, 659 (1967) (19.5 MeV).
- ²⁹G. A. Proca and D. B. Isabelle, Nucl. Phys. A109, 177 (1968) (15.1, 16.1, 18.9, 20.3, 16.6, 19.4, 20.9, 22.2 MeV).
- ³⁰G. A. Beer, T. E. Drake, R. M. Hutcheon, V. W. Stobie, and H. S. Caplon, Nuovo Cimento 53B, 7 (1968) (19.4 MeV).
- ³¹T. W. Donnelly, J. D. Walecka, I. Sick, and E. B. Hughes, Phys. Rev. Letters 21, 1196 (1968).
- ³²The oscillator expressions for the 15.11-, 16-, and 19-MeV levels and the "giant resonance" were obtained in a private communication with T. W. Donnelly.
- ³³For a discussion of nucleon form factors, see, J. G. Rutherglen, in *International Symposium on Electron and Photon Interactions at High Energies, Liverpool, Eng- land, 1969*, edited by D. W. Braben (Daresbury Nuclear Physics Laboratory, Daresbury, Lancashire, England, 1970), p. 163.
- ³⁴J. E. Leiss and R. E. Taylor, in Karlsruhe Photonuclear Conference, 1960 (to be published). These data are quoted by Refs. 7 and 36.
- ³⁵D. Isabelle and H. W. Kendall, Bull. Am. Phys. Soc. 9, 95 (1964).
- ³⁶P. D. Zimmerman, Ph.D. thesis, Stanford University, 1969 (unpublished).
- ³⁷U. Amaldi, Jr., G. Campos Venuti, G. Cortellessa, C. Fronterotta, A. Reale, P. Salvadori, and P. Hillman, Phys. Rev. Letters 13, 341 (1964).
- ³⁸U. Amaldi, Jr., G. Campos Venuti, G. Cortellessa, F. De Sanctus, S. Frullani, R. Lombard, and P. Salva- dori, Phys. Letters 25B, 24 (1967).
- ³⁹W. Czyz, Phys. Rev. 131, 2141 (1963).
- ⁴⁰G. R. Henry, Phys. Rev. 151, 875 (1966).
- ⁴¹G. R. Henry, Phys. Rev. 157, 871 (1967).
- ⁴²T. de Forest, Jr., Nucl. Phys. A132, 305 (1969).
- ⁴³A. Małecki and P. Picchi, Nuovo Cimento 58A, 145 (1968).
- ⁴⁴J. Løvseth, Nuovo Cimento 57A, 782 (1968).
- ⁴⁵T. W. Donnelly, Nucl. Phys. A150, 393 (1970).
- ⁴⁶T. de Forest, Jr., Ann. Phys. (N.Y.) 45, 365 (1967).
- ⁴⁷G. Henry, private communication.
- ⁴⁸W. Czyz and J. D. Walecka, Nucl. Phys. 51, 312 (1964).
- ⁴⁹S. Fubini, Y. Nambu, and V. Wataghin, Phys. Rev. 111, 329 (1958).
- ⁵⁰A. J. Dufner and Y. S. Tsai, Phys. Rev. 168, 1801 (1968).
- ⁵¹M. Gourdin and Ph. Salin, Nuovo Cimento 27, 193 (1963).
- ⁵²M. Gourdin and Ph. Salin, Nuovo Cimento 27, 300 (1963).
- ⁵³J. D. Jackson, Nuovo Cimento 24, 1644 (1964).
- ⁵⁴L. Mo and Y. S. Tsai, Rev. Mod. Phys. 41, 205 (1969).
- ⁵⁵J. Tenebaum, A. M. Eisner, G. J. Feldman, W. Lock- erez, F. M. Pipkin, and J. K. Randolph, Phys. Rev. D 2, 57 (1970).
- ⁵⁶J. K. Randolph, A. M. Eisner, G. J. Feldman, W. Lockeretz, F. M. Pipkin, and J. Tenebaum, Phys. Rev. D 2, 1852 (1970).
- ⁵⁷W. T. Scott, Rev. Mod. Phys. 35, 231 (1963).
- ⁵⁸L. N. Hand, Phys. Rev. 129, 1834 (1963).
- ⁵⁹W. Bartel, B. Dudelzak, H. Krehbiel, J. McElroy, V. Meyer-Berkhout, W. Schmidt, V. Walther, and G. Weber, Phys. Letters 28B, 148 (1968).
- ⁶⁰F. W. Brasse, J. Engler, E. Gansauge, and M. Sch- weizer, Nuovo Cimento 55A, 679 (1968).
- ⁶¹A. A. Cone, K. W. Chen, J. R. Dunning, G. Hartwig, N. Ramsey, J. K. Walker, and R. Wilson, Phys. Rev. 156, 1490 (1967).
- ⁶²H. L. Lynch, J. V. Allaby, and D. M. Ritson, Phys. Rev. 164, 1635 (1965).
- ⁶³G. Ohlsen, Phys. Rev. 120, 584 (1960).
- ⁶⁴W. Panofsky and E. Allton, Phys. Rev. 110, 1155 (1958).
- ⁶⁵S. D. Drell and C. L. Schwartz, Phys. Rev. 112, 568 (1958).
- ⁶⁶For a related sum rule see K. W. McVoy and L. Van Hove, Phys. Rev. 125, 1034 (1962).